

1 **REVISION 1**

2 **Interlayer water molecules in organocation-exchanged vermiculite and**
3 **montmorillonite: A case study of tetramethylammonium**

4
5 Ruben Martos-Villa¹, Stephen Guggenheim², C. Ignacio Sainz-Díaz^{3*}

6
7 ¹ Facultad de Ciencias del Mar y Ambientales, Universidad de Cádiz, Av. República
8 Saharaui s/n, 11510 Puerto Real, Spain.

9 ² University of Illinois at Chicago, 845 W. Taylor St., Chicago, Illinois 60607, U. S. A.

10 ³ Instituto Andaluz de Ciencias de la Tierra, CSIC-Universidad de Granada, Av. de las
11 Palmeras, 4, 18100-Armilla, Granada, Spain. cisainz@ugr.es

12
13 **ABSTRACT**

14 Organoclays, unlike natural clays with inorganic cations that often have a hydration
15 shell of H₂O molecules, become organophilic and less adsorptive of H₂O. These clays,
16 therefore, are potentially important to remove organic contaminants from water; they are of
17 great interest in industry for herbicide manufacture and as the basis for nanocomposite
18 development; and they are of general interest in agriculture and in understanding soils.
19 However, nothing is known about the positions of H₂O in the interlayer when these
20 molecules intercalate along with medium-sized hydrocarbon molecules, such as
21 tetramethylammomium (TMA) cations. Even the positions of the TMA cations in the
22 interlayer have been questioned recently. To resolve these issues, the orientation and

23 position of TMA and H₂O in the interlayer of vermiculite and montmorillonite were
24 investigated by using atomistic computational methods. Interlayer H₂O content, layer
25 charge, and location of layer charge were considered. For both vermiculite and
26 montmorillonite and where the number of H₂O molecules is sufficient, TMA cations are
27 located alternating between two planes in the interlayer. Each TMA cation is located near a
28 tetrahedral-ring cavity of a 2:1 layer bordering the interlayer, and the H₂O molecules are
29 disordered. In the absence of H₂O, TMA cations occur in one plane at the center of the
30 interlayer. The major difference between vermiculite and montmorillonite is that the center
31 of the TMA molecule in montmorillonite is 0.87 Å from the center of the interlayer as
32 compared to 1.22 Å in vermiculite. Thus, the TMA cation is located closer to the
33 tetrahedral-ring cavity in vermiculite, and this is a result of the greater tetrahedral charge of
34 vermiculite. In fluorohectorite, which is similar in layer charge and origin of layer charge as
35 the montmorillonite composition studied, the position of the TMA is expected to be similar
36 to the montmorillonite results. These computational models are consistent with single
37 crystal, X-ray diffraction experiments for hydrated TMA-exchanged vermiculite and dried
38 fluorohectorite.

39

40 **Keywords:** interlayer cation and H₂O positions, swelling clay minerals, layer charge,

41 phyllosilicates, layer silicates, computational mineralogy

42 INTRODUCTION

43 The swelling clay minerals, smectite and vermiculite, are deficient in positive layer
44 charge because of cation substitutions either in the octahedral sheet (e.g., Mg^{2+} for Al^{3+}),
45 tetrahedral sheet (e.g., Al^{3+} for Si^{4+}) or both sheets (e.g., Brigatti et al., 2011 for a summary).
46 To offset this charge deficiency, the common exchangeable cations in nature (e.g., K, Na,
47 Mg, Fe) may enter the interlayer along with H_2O molecules (Bailey, 1980). However, an
48 exchangeable cation may also be an “organic cation” (e.g., any charged hydrocarbon
49 molecule), and these clays generally are less adsorptive of H_2O and instead become more
50 organophilic (Johnston, 1996; Cadena and Cazares, 1996 for summaries). Thus, the
51 organoclays not only become important to remove organic contaminants from water, but
52 they are important also in understanding agriculture and soils in general and herbicides
53 specifically (Boyd and Jaynes, 1994). Tetra-alkylammonium (e.g. tetramethylammonium)
54 salts have been used to produce organoclays in the last few decades, acting as surfactants
55 with polar features (ammonium groups) and an apolar moiety (alkyl groups). These apolar
56 groups increase the lipophilic character of the interlayer, and the adsorption capacity of
57 organic molecules increases significantly (Lee et al. 1990). In addition, organic cations (or
58 polar molecules) intercalated in a fixed orientation within the interlayer can also form the
59 basis of nanocomposites. However, little is known about the positions of H_2O in the
60 interlayer, and even the position of the hydrocarbon molecule has been called into question.
61 This paper combines structure information from experiment and simulation techniques to
62 determine where H_2O molecules reside in the interlayer of swelling clay minerals with

63 limited hydrophobicity. Furthermore, the simulations explain apparent discrepancies
64 between some of the experimental data.

65

66 Smectite and vermiculite are group names of two different clay mineral groups
67 closely related in structure (Bailey, 1980). The general formula for smectite,
68 unconventionally written, is $\sim[X_{0.3} \cdot nH_2O]^+ [Y_{2-3}Z_4O_{10}(OH)_2]^-$, where X is an exchangeable
69 cation, Y is a small- to medium-sized, octahedrally coordinated cation that is trivalent in
70 charge if the subscript is 2.0 (= dioctahedral) or divalent if the subscript is 3.0 (=
71 trioctahedral), Z is a small tetrahedrally-coordinated cation (usually Si^{4+} or Al^{3+}), and n may
72 be variable. The structural formula for vermiculite, in an analogously written formula, is
73 $\sim[X_{0.5} \cdot nH_2O]^+ [Y_{2-3}Z_4O_{10}(OH)_2]^-$, where n is near 4 and the other symbols are the same as
74 those defined for smectite (Bailey, 1988). Both groups have 2:1 layers (the negative part of
75 each formula) consisting of an octahedral sheet between two tetrahedral sheets, with the
76 latter sheets inverted relative to each other. They are mineralogically differentiated by their
77 2:1 layer charge, with smectites having a layer charge per formula unit of approximately -0.2
78 to -0.6 (or -0.4 to -1.2 per unit cell) and vermiculites with -0.6 to -0.9 (Bailey 1980). Layer
79 charge is important because cation-exchange properties, absorption properties, and physical
80 properties are greatly affected by small changes in layer charge and by the location of the
81 layer charge (either in tetrahedra or octahedra, or both). Exchange and adsorption
82 commonly occur between the 2:1 layers, known as the interlayer, or on sites at the broken
83 edges of the particles, but these latter sites are not considered here. Within each group,
84 chemical differences separate the different mineral species.

85

86 The understanding of the reactivity of organic solutes with such clay minerals
87 requires knowledge of the chemistry and structure of the mineral. Unfortunately, owing to
88 the high degree of 2:1 layer stacking disorder (in smectite and vermiculite) and very small
89 particle size (in smectite), the complete characterization of the crystal structure based on
90 conventional diffraction analysis is extremely difficult, but several approaches have been
91 used to facilitate diffraction studies. The tetramethylammonium (TMA) cation does not
92 produce a high hydrophobicity to the interlayer because the alkyl groups are relatively small.
93 In addition, the TMA cation in the interlayer facilitates the cross linking of adjacent layers to
94 promote stacking order. Combining these materials with TMA intercalation allows
95 sufficiently large crystals to be analyzed by single-crystal X-ray diffraction techniques
96 (Vahedi-Faridi and Guggenheim 1997). Therefore, structural studies have been possible
97 using both experimental and simulation techniques for comparison.

98

99 Vahedi-Faridi and Guggenheim (1997) obtained a structure model of TMA-
100 exchanged natural vermiculite from Santa Olalla, Spain (trioctahedral, layer charge
101 primarily originates from tetrahedra, layer charge = -0.85), by single-crystal X-ray
102 diffraction (XRD). They proposed a model (Fig. 1) based on XRD data where the TMA
103 cations are located offset from the center plane of the interlayer by 1.52 Å and one C atom
104 of the TMA tetrahedron is keyed into the silicate tetrahedral-ring cavity. Thus, the TMA
105 cations are arranged with their C_3 axis perpendicular to the silicate 2:1 layer, with one face
106 of the NC_4 tetrahedron (centered by the N atom and surrounded by the C atoms at the

5

107 vertices) parallel to the silicate layers. Each N atom site has an occupancy of 41.8% if all
108 possible positions are occupied, and the TMA cations form two planes within the interlayer
109 where the TMA cations are alternating between these planes. The X-ray study made no
110 assumptions about the interlayer structure, and used difference maps and electron density
111 profiles (Fourier techniques) to derive the structure of the interlayer. Using theoretical
112 studies based on empirical interatomic potentials for vermiculite of similar composition,
113 Čapková et al. (1999) reported that the TMA cations occurred in only the plane at the
114 interlayer center with one of the C-C edges of the NC_4 tetrahedra perpendicular to the layers.
115 This model is clearly contradictory with the electron density profile of the XRD study.

116

117 Seidl and Breu (2005) studied a synthetic Li- and F-rich smectite (trioctahedral, layer
118 charge originates in octahedra, layer charge = -0.5), fluorohectorite, by single-crystal XRD
119 after TMA exchange. In fluorohectorite, TMA cations are essentially in the center plane of
120 the interlayer, in accord with the Čapková et al. (1999) model. Moreover, the C_3 axis of
121 TMA is not perpendicular to the silicate layers, but tilted towards the (001) plane. However,
122 one C-C edge of the NC_4 tetrahedron is perpendicular to the (001) plane. Consequently, the
123 apical methyl group is shifted away from the middle of the tetrahedral-ring cavity to one
124 side (Fig. 1). Because the electron density of the interlayer was highly diffuse (Seidl and
125 Breu 2005), the TMA was treated as a rigid body.

126

127 Two other smectites, montmorillonite (dioctahedral, layer charge originates in the
128 Al- and Mg-rich octahedral sheet) and beidellite (dioctahedral, layer charge originates in the

129 Al-rich tetrahedral sheet), were examined considering the layers and TMA cations as rigid
130 units without optimizations and using empirical interatomic potentials by Čapková et al.
131 (2000), with a layer charge of -0.475 and -0.6, respectively. Two possible TMA models for
132 each smectite were presented. Model 1 has TMA in projection within the silicate tetrahedral
133 rings, but with every alternate 6-ring chain occupied. Model 2 has some TMA projecting on
134 top of silicate tetrahedra and others partially over the silicate tetrahedral rings. Both models
135 indicated that TMA were located on the central plane of the interlayer. Supporting
136 experimental structural data were not presented, and these models are not discussed in detail
137 further.

138

139 Vahedi-Faridi and Guggenheim (1997) heat-treated the sample to 250 °C after
140 structural analysis that resulted in a decrease in $d(001)$ value of 0.37 Å, which indicated the
141 presence of H₂O in the crystal although there was no apparent XRD scattering from H₂O
142 present in the data. Based on these results, they suggested that interlayer H₂O is disordered
143 in the structure. In contrast, Seidl and Breu (2005) took great care to dehydrate their crystal
144 before analysis by drying in a high vacuum for 4 days at 90 °C and immersing in
145 perfluorether to prevent rehydration. The theoretical studies by Čapková et al. (1999, 2000)
146 did not consider the possible effects of interlayer H₂O.

147

148 The fundamental assumption apparently used by Seidl and Breu (2005) in their study
149 was that only one structural model must be correct for TMA-exchanged fluorohectorite vs.
150 vermiculite. In contrast, we assume that both models may possibly be correct and that the

151 reason for the structural discrepancies requires further clarification. There are many
152 possible parameters to consider that may cause these discrepancies, and they include
153 differences in layer charge, interlayer H₂O content (including effects of relative humidity),
154 synthetic vs. natural starting material (and possible short-range cation order and layer
155 stacking differences), compositional differences (in the tetrahedra, octahedra, and
156 interlayer), sample preparation differences, and others. The present paper considers
157 interlayer H₂O content, total layer charge, and location of layer charge, by using quantum
158 mechanical calculations to model the structures of vermiculite and montmorillonite. These
159 models have implications to understand the fluorohectorite results of Seidl and Breu (2005).

160

161 **Computational Methods**

162 *Calculation procedures*

163 Quantum mechanical calculations of an isolated TMA cation were performed using
164 the Hartree-Fock (HF) approximation including the second-order Moeller-Plesset (MP2)
165 method for describing the electron exchange correlation for all electrons. The molecular
166 electronic structure was calculated with a triple- ζ basis set with polarization functions for all
167 atoms including H atoms (MP2/6-311G** level) as implemented in the Gaussian03 program
168 (Frisch et al. 2004). No geometry constraint was applied to the molecule, which was fully
169 optimized using the Bery analytical gradient method. Normal vibration modes were
170 calculated from the force-constant analysis to confirm the nature of the stationary points,
171 which resulted in only positive eigenvalues for the minimum.

172

173 *Ab initio* total energy calculations of the periodic crystal model were performed
174 using density functional theory (DFT) methods based on the numerical atomic orbital
175 (NAO) methodology implemented in the SIESTA program (Soler et al. 2002). The
176 generalized gradient approximation (GGA) was used with the Perdew-Burke-Ernzerhof
177 (PBEsol) parameterization of the exchange-correlation function optimized for solids
178 (Perdew et al. 2008). Core electrons were replaced by norm-conserving pseudopotentials
179 (Troullier and Martins 1991). Calculations were restricted to the Γ point in the irreducible
180 wedge of the Brillouin zone. In all structures, the geometry of each atom was relaxed by
181 means of conjugated gradient optimizations at constant experimental volume. In SIESTA,
182 the basis sets are made of strictly localized numerical atomic orbitals (NAOs) with a
183 localization cut-off radius corresponding to an energy shift of 270 meV. The basis sets used
184 here are double-Z polarized (DZP) following the perturbative polarization scheme. This
185 approach was successfully used in previous calculations on phyllosilicates (Hernández-
186 Laguna et al. 2006).

187

188 A uniform mesh with appropriate plane-wave cut-off energy is used to represent the
189 electron density, the local part of the pseudopotential, and the Hartree and exchange-
190 correlation potentials. Total energy calculations were performed with cut-off energy values
191 of 150 Ry. These conditions are consistent with previous studies with phyllosilicates (Sainz-
192 Díaz et al. 2005).

193

194 *Model development*

195 Model development involved defining each component of the phyllosilicate and then
196 assembling these components. Analyses were made using increasingly complex
197 assemblages.

198 *The basic 2:1 layer.* A periodic model of the crystal structure of vermiculite was
199 generated from the experimental atomic coordinates and cell parameters given in Vahedi-
200 Faridi and Guggenheim (1997). To create a supercell of a reasonable size for modeling, the
201 structural formula of the vermiculite 2:1 layer used in the modeling experiments was
202 simplified to the form: $(\text{Mg}_{5.25}\text{Al}_{0.75})(\text{Si}_{5.5}\text{Al}_{2.5})\text{O}_{20}(\text{OH})_4$ per unit cell, where the layer
203 charge per unit cell is -1.75 (LC models). Additional models with very low charge (-1.25)
204 $(\text{Mg}_5\text{Al})(\text{Si}_{5.75}\text{Al}_{2.25})\text{O}_{20}(\text{OH})_4$ (VLC models) and high charge (-2) $(\text{Mg}_{5.5}\text{Al}_{0.5})(\text{Si}_{5.5}\text{Al}_{2.5})\text{O}_{20}$
205 $(\text{OH})_4$ (HC models) were generated by adjusting the chemical composition of the layer
206 (Table 1). Maximum separations between cation substitutions in the tetrahedral and
207 octahedral sheets are used because these configurations are more stable based on previous
208 calculations (Palin et al. 2004; Sainz-Díaz et al. 2003). Each model consisted of a supercell
209 of 2 x 2 x 1 vermiculite subcells (Fig. 2). To compensate the layer charge in this supercell,
210 TMA cations, previously optimized by quantum mechanical calculations, were placed in the
211 supercell to explore the different possible arrangements in the interlayer.

212

213 *Models involving intercalated TMA.* The TMA cation was obtained from atomic
214 coordinates extracted from XRD data (Vahedi-Faridi and Guggenheim 1997) and initially
215 optimized at MP2/6-311G** level and later reoptimized using the DFT-SIESTA approach
216 before intercalation. Within the 2 x 2 x 1 supercell, HC models (Fig. 2) were further defined

217 as an HC1 model consisting of eight TMA cations located with each having one methyl
218 group in the center of the tetrahedral-ring cavities, placing alternating four TMA cations
219 near the lower silicate layer and four TMA cations near the upper silicate layer. For each
220 model, TMA positions were adjusted depending on the location of the local charge in the
221 layer. The HC2 model is similar to the HC1 model, but four TMA cations are arranged
222 such that two TMA pairs are located in the same *ab* site, where the centroids of the cations
223 have the same *x* and *y* values but with different *z* coordinate values forming two-TMA
224 pillars; in HC3, all TMA cations form pairs in the same *ab* site with different *z* coordinate
225 values, but in the four central cavities of the supercell. The HC4 model is similar to HC2 but
226 three TMA cations are located to form two-TMA pillars. In each LC model, there are seven
227 TMA cations per supercell of vermiculite; three TMA cations are located within the upper-
228 layer tetrahedral-ring cavity and four cations in the lower-layer, alternately located in the
229 tetrahedral-ring cavities with greatest local charge, and one pair of cavities is without TMA.
230 In the VLC models, the five TMA cations are located as in HC1 (VLC1) or forming pairs
231 alternately as in HC2 (VLC2).

232 *Models involving H₂O + TMA.* Different numbers of H₂O molecules were added to
233 TMA-vermiculite models in a disordered fashion. In each case, there are seven TMA cations
234 and eight pairs of tetrahedral-ring cavities per 2x2x1 supercell (simulation cell). The cavity
235 pair without TMA is filled with more H₂O molecules than the cavity pair with each TMA.
236 For example, the LC-W1 model has 9 water molecules per simulation cell: one H₂O
237 molecule is located in each cavity at the opposite site to each TMA and two water molecules
238 are located in the cavity without TMA (4.4 % w/w of total water content); LC-W2 has 18

239 water molecules per simulation cell: same as LC-W1, but adding two H₂O molecules per
240 TMA and four water molecules in the cavity without TMA (9.2 % total water content); LC-
241 W3 has 27 water molecules per simulation cell: adds three H₂O molecules per TMA and six
242 water molecules in the cavity without TMA (12.0 % total water content); LC-W4 has 34
243 water molecules per simulation cell: adds four H₂O molecules in each tetrahedral-ring cavity
244 opposite from each TMA site and six water molecules in the cavity without TMA (14.5 % of
245 water) (Table 1). All water molecules were placed randomly to avoid electrostatic
246 repulsions.

247 In addition, a montmorillonite model with TMA was also studied as a model with
248 octahedral charge, but without tetrahedral charge, [TMA · 8H₂O]⁺ [(Al₃Mg)(Si₈)O₂₀(OH)₄]⁻,
249 with 8 water molecules per unit cell. In this model with low interlayer charge, only one
250 cavity is occupied by TMA and 4 water molecules are located between the TMA and the
251 other adjacent tetrahedral sheet. The tetrahedral-ring cavity without TMA is filled with 4
252 water molecules.

253

254 **RESULTS**

255 *TMA molecule.* The molecular structure of TMA as a gas was analyzed after
256 optimizing at MP2/6-311G**, and DFT levels. The latter also included optimizing the TMA
257 molecule in an isolated periodic box. Each method reproduced the experimental values
258 (Vahedi-Faridi and Guggenheim 1997) of H-C-N and C-N-C angles (109°-109.5°), and C-N
259 (1.47-1.50 Å) and C-H (1.09-1.12 Å) bond lengths.

260

261 *TMA-intercalated vermiculite structures.* In the optimization calculations of the
262 HC1 model, all TMA cations are displaced to the center plane of the interlayer region with
263 the C_3 axis no longer perpendicular to the silicate layers but tilted towards the *ab*-plane as in
264 the model of Seidl and Breu (Fig. 3a). In the HC2 and HC4 models, initially one TMA
265 molecule is located near the upper tetrahedral-ring cavity and alternately one TMA molecule
266 is located near the lower ring cavity as in HC1; however, in these models this arrangement
267 produces some TMA cations that form two-TMA pillars. In the optimized structures these
268 latter TMA cations are located in two levels of the interlayer as two-TMA pillars (Fig 3b)
269 and the remaining TMA cations are displaced to the center plane of the interlayer region
270 with the C_3 axis no longer perpendicular to the silicate layers but tilted towards the *ab*-plane
271 as in the model of Seidl and Breu. In calculations involving HC3, all TMA cations are
272 located forming pillars (4 keyed in the upper layer and 4 keyed in the lower layer).
273 Geometry optimizations maintain all TMA cations oriented in two planes in the interlayer
274 maintaining the pillars (Fig. 3c). The HC1 structure is the most stable of these models and
275 the two-TMA pillars produce a high instability to the complex (Table 1). The same behavior
276 was observed in the VLC models with lower interlayer charge, where VLC1 is more stable
277 than VLC2 (Table 1).

278 *Intercalations of TMA + H₂O in vermiculite.* In all optimized models with water, the
279 water molecules appear disordered. Geometry optimizations in LC-W1 and LC-W2 models
280 yielded shifts of TMA cations, where TMA cations are rotated and located in the central
281 plane of the interlayer, similar to the dry TMA-exchanged vermiculite structure. The water
282 molecules form H bonding to each other and to the basal tetrahedral O atoms. For LC-W1,

283 water molecules are in the tetrahedral cavities and do not interact with TMA cations. The H-
284 O-H plane is parallel to the (001) plane and H bonds form between the water-molecule H
285 atoms and the O atoms of the basal tetrahedral plane and between the water-molecule O
286 atoms and the H atom of the OH group in the octahedral sheet. The orientation of the O-H
287 vector in the octahedral sheet has an inclination ρ angle of 90° with respect to the (001)
288 plane. In the LC-W3 model, geometry optimization produced a pattern where TMA cations
289 alternate in two planes in the interlayer. However, these TMA cations are not located with
290 the C atom in the tetrahedral-ring cavity and most are rotated. The water molecules are
291 connected forming a H bonding network between TMA and the basal tetrahedral O atoms.
292 Finally, optimization of the LC-W4 model resulted in two planes of TMA cations with the C
293 atom keyed to the tetrahedral-ring cavity to reproduce the model of Vahedi-Faridi and
294 Guggenheim (Fig. 4a). The H atoms of the methyl groups of TMA, which are close to the
295 tetrahedral-ring cavity, form H bonds with the basal oxygen atoms with distances of 1.77 –
296 1.93 Å. Water molecules form a H bonding network with other water molecules and also
297 strong H bonds with basal tetrahedral oxygen atoms (1.65-1.43 Å) as well as with the
298 octahedral OH groups (1.38 Å between the O atom of H₂O and the H atom of the OH group
299 within the octahedral sheet).

300 *Intercalations of TMA + H₂O in montmorillonite.* The main difference between
301 vermiculite and hectorite is the lower tetrahedral charge in hectorite than in vermiculite.
302 Hence, a model of montmorillonite without tetrahedral charge was chosen, to explore the
303 effect of the tetrahedral charge in the disposition of TMA in the interlayer. The optimization
304 of both models, with 8 water molecules per unit cell, yielded the TMA molecule displaced

305 from the interlayer center. The TMA molecule is close to one tetrahedral-ring cavity and
306 some water molecules are between the TMA and the opposing side of the interlayer. This
307 disposition is similar to that observed in vermiculite. However, in montmorillonite the
308 methyl group is oriented to the tetrahedral-ring cavity such that it is less anchored to this
309 cavity than in vermiculite (Fig. 4b). For example, the H atoms of the methyl groups of
310 TMA, which are close to the tetrahedral-ring cavity, form weaker interactions with the basal
311 tetrahedral O atoms (1.99 – 2.26 Å) than in vermiculite. Water molecules are disordered and
312 no water molecule was found trapped in the tetrahedral cavities.

313

314 **Discussion**

315 *The effect of H₂O in TMA-exchanged vermiculite.* The number of disordered water
316 molecules has a critical role in the crystal structure of this organo-exchanged clay mineral.
317 Where there are a sufficient number of water molecules, TMA cations are located alternating
318 in two planes, which is consistent with the Vahedi-Faridi and Guggenheim model. However,
319 in the absence of water molecules, TMA cations are distributed in one plane at the center of
320 the interlayer (Fig 5a), as found by Seidl and Breu (2005) in hectorite and modeled in
321 vermiculite and montmorillonite by Čapková et al. (1999, 2000). Because of the high
322 hygroscopicity of TMA, the presence of water molecules in the interlayer is probably the
323 case for most samples, unless special effort is made to dehydrate the material.

324

325 With the presence of only one water molecule per TMA cation, an asymmetry in the
326 density profile of N atoms along the [001] direction is observed (Fig. 5b). However, the

327 TMA cations are mainly in the interlayer center because the water molecules are trapped in
328 the tetrahedral cavity with high tetrahedral charge and they do not interact with the TMA
329 cations. In the LC-W4 structure the TMA cations are surrounded by water molecules
330 forming a cage. This cage is similar to a clathrate hydrate where the basal oxygen atoms of
331 the closest tetrahedral-ring cavity act as coordinated water molecules completing the
332 hydration cage. Similar cages are observed experimentally in hydrates of TMA hydroxide
333 (Ratcliffe et al. 1990). In our case, the anion is the negative charge provided by the 2:1 layer,
334 and the basal oxygen atoms of the 2:1 layer form a hexagonal face of the hydrate cage.
335 Nevertheless, a hydrophobic zone occurs between the methyl groups with no water
336 molecules associated with the TMA cations.

337 The shift of the N atom (as a center of the TMA molecule) with respect to the
338 interlayer center (1.22 Å, Fig. 5a) indicates than the TMA position is not only related to the
339 tetrahedral charge but also to the H bonds between the methyl H atoms and the basal oxygen
340 atoms of the tetrahedra.

341 Where water molecules are randomly distributed in the interlayer, however, there is
342 local ordering as observed in the density profile of the O atoms of water molecules along the
343 [001] direction in the interlayer space. Two peaks are observed for the O atoms in a similar
344 way as to the N atoms of the TMA cations. This indicates that the water molecules occupy
345 the space vacated by the TMA shift from the interlayer center. Nevertheless, these peaks are
346 wider and with lower relative intensity with respect to the vermiculite peaks density than
347 those of the N atoms of TMA cations owing to the high disorder of the water molecules.
348 Two additional peaks are observed at the same level of the basal oxygen atoms of the

349 tetrahedra indicating the strong interaction of one water molecule with the O atoms of the
350 cavity formed within the tetrahedral ring and the octahedral hydroxyl group (Fig. 6).
351 Considering the radial distribution function of the water molecule atoms in the interlayer
352 with TMA cations, the O...O, H...H and O...H distances are slightly shorter than in other
353 hydrates (Martos-Villa et al. 2013) probably owing to the confined space of the vermiculite
354 interlayer (Fig. 6).

355

356 *Effect of H₂O in TMA-exchanged montmorillonite.* The asymmetry of the TMA
357 cations with respect to the interlayer center observed in vermiculite is apparently attributed
358 to the relatively high charge of vermiculite originating from substitutions in tetrahedral sites.
359 However, this asymmetry is also observed to a lesser degree in the montmorillonite model
360 with no tetrahedral charge. This asymmetry is smaller than in vermiculite, owing to the
361 weaker interactions between the methyl H atoms of TMA and the basal oxygen atoms of the
362 tetrahedra. Consequently, the C-N bond of the methyl group oriented towards the
363 tetrahedral-ring cavity does not have the perpendicular orientation with respect to the
364 tetrahedral sheet, unlike the arrangement that occurs in vermiculite. The shift of the N atom
365 of TMA with respect to the center of the interlayer is 0.87 Å (Fig. 5c), which is smaller than
366 that observed in vermiculite (1.22 Å) (Fig. 5a). In this case, the water molecules do not
367 interaction with the tetrahedral cavities so strongly as in the vermiculite samples due to the
368 lack of the tetrahedral charge and the inclination of the octahedral OH group which is not
369 oriented towards the interlayer.

370

371 Quantum mechanical calculations are capable of clarifying why differences occur
372 between the hydrous and anhydrous TMA models of vermiculite, montmorillonite and
373 fluorohectorite. However, such an analysis requires that all reasonable models need to be
374 anticipated when developing a theoretical study, and thus it is especially useful to combine
375 both theoretical and experimental approaches.

376

377 ACKNOWLEDGMENTS

378 Funding for this work was obtained from the Junta de Andalucía RNM-3581
379 CADHYS project. The authors thank P. Mata for her useful discussions, and to the
380 Supercomputational Center of the Granada University (UGRGRID) and to the Centro
381 Técnico de Informática del CSIC.

382

383 **References**

384 Bailey, S.W. (1980) Structures of layer silicates, in: Crystal structures of clay minerals and
385 their X-ray identification, edited by G.W. Brindley and G. Brown, pp. 1-124, Mineralogical
386 Society (of Great Britain), London.

387

388 Bailey, S.W. (Ed.) (1988) Hydrous Phyllosilicates, Reviews in Mineralogy vol. 19,
389 Mineralogical Society of America, BookCrafters, Chelsea, Michigan.

390

391 Boyd, S.A. and Jaynes, W.F. (1994) Role of layer charge in organic contaminant sorption by
392 organo-clays. In CMS Workshop Lectures, 6, 47-78, Mermut, A.R., Ed., The Clay Minerals
393 Society, Aurora, CO, USA.

394

395 Brigatti, M.F., Malferrari, D., Laurora, A., and Elmi, C. (2011) Structure and mineralogy of
396 layer silicates: recent perspectives and new trends. In EMU Notes in Mineralogy, 11, 1-71,
397 Brigatti, M.F. and Mottana, A., Eds. European Mineralogical Union and the Mineralogical
398 Society of Great Britain, London.

399

400 Cadena, F. and Cazares, E. (1996) Use of organozeolites for the removal of organic
401 contaminants from water. In CMS Workshop Lectures, 8, 69-94, Sawhney, B.L., Ed., The
402 Clay Minerals Society, Boulder, CO, USA.

403

404 Čapková, P., Burda, J.V., Weiss, Z., and Schenk, H. (1999) Modelling of aniline-
405 vermiculite and tetramethylammonium-vermiculite; Test of force fields. Journal of
406 Molecular Modeling, 5, 8-16.

407

408 Čapková, P., Pospíšil, M., Miehé-Brendlé, J., Trchová, M., Weiss, Z., and Le-Dred, R.
409 (2000) Montmorillonite and Beidellite Intercalated with Tetramethylammonium cations.
410 Journal of Molecular Modeling, 6, 600 – 607.

411

412 Frisch, M.J., Trucks, G.W., Schlegel, H.B., Scuseria, G.E., Robb, M.A., Chesseman, J.R.,
413 Zarzewski, V.G., Montgomery, J.A., Stratmann, R.E., Burant, J.C., Dapprich, S., Millam,
414 J.M., Daniels, A.D., Kudin, K.N., Strain, M.C., Farkas, O., Tomasi, J., Barone, V., Cossi,
415 M., Cammi, R., Mennucci, B., Pomelli, C., Adamo, C., Clifford, S., Ochterski, J., Petersson,
416 G.A., Ayala, P.Y., Cui, Q., Morokuma, K., Malick, D.K., Rabuck, A.D., Raghavachari, K.,
417 Foresman, J.B., Cioslowski, J., Ortiz, J.V., Stefanov, B.B., Liu, G., Liashenko, A., Piskorz,
418 P., Komaromi, I., Gomperts, R., Martin, R.L., Fox, D.J., Keith, T.A., Al-Laham, M.A.,
419 Peng, C.Y., Nanayakkara, A., Gonzalez, C., Challacombe, M., Gill, P.M.W., Johnson, B.G.,
420 Chen, W., Wong, M.W., Andres, J.L., Head-Gordon, M., Replogle, E.S., and Pople, J.A.
421 (2004). Gaussian 03 (RevisionA.1), Gaussian, Inc., Pittsburgh, PA.

422

423 Hernández-Laguna, A., Escamilla-Roa, E., Timón, V., Dove, M.T., and Sainz-Díaz, C.I.
424 (2006) DFT study of the cation arrangements in the octahedral and tetrahedral sheets of
425 dioctahedral 2:1 phyllosilicates. Physics and Chemistry of Minerals, 33, 655-666.

426

427 Johnston, C.T. (1996) Sorption of organic compounds on clay minerals: A surface functional
428 group approach. In CMS Workshop Lectures, 8, 1-44, Sawhney, B.L., Ed., The Clay
429 Minerals Society, Boulder, CO, USA.

430

431 Lee, J., Mortland, M.M., Chiou, C.T., Kile, D.E., and Boyd, S.A. (1990) Adsorption of
432 benzene, toluene, and xylene by two tetramethylammonium-smectites having different
433 charge densities. *Clays and Clay Minerals*, 38, 113-120.

434

435 Martos-Villa, R., Francisco-Márquez, F., Mata, P., and Sainz-Díaz, C.I. (2013). Crystal
436 structure, stability and spectroscopic properties of methane and CO₂ hydrates. *Journal of*
437 *Molecular Graphics and Modelling* (submitted).

438

439 Palin, E.J., Dove, M.T., Hernández-Laguna, A., and Sainz-Díaz, C.I. (2004) A
440 computational investigation of the Al/Fe/Mg order-disorder behavior in the dioctahedral
441 sheet of phyllosilicates. *American Mineralogist*, 89, 164-175.

442

443 Perdew, J.P., Ruzsinszky, A., Csonka, G.I., Vydrov, O.A., Scuseria, G.E., Constantin, L.,
444 Zhou, X., and Burke, K. (2008) Restoring the Density-Gradient Expansion for Exchange in
445 Solids and Surfaces, *Physical Review Letter*, 100, 136406.

446

447 Ratcliffe, C.I., Garg, S.K., and Davidson, D.W. (1990) NMR Studies of Molecular Motion
448 in Tetramethylammonium Hydroxide Pentahydrate. *Journal of Inclusion Phenomena and*
449 *Molecular Recognition in Chemistry*, 8, 159-175.

450

451 Sainz-Díaz, C. I., Palin, E.J., Hernández-Laguna, A., and Dove, M.T. (2003) Octahedral
452 cation ordering of illite and smectite. Theoretical exchange potential determination and
453 Monte Carlo simulations. *Physics and Chemistry of Minerals*, 30, 382-392.

454

455 Sainz-Díaz, C.I., Escamilla-Roa, E., and Hernández-Laguna, A. (2005) Quantum mechanical
456 calculations of trans-vacant and cis-vacant polymorphism in dioctahedral 2:1 phyllosilicates.
457 *American Mineralogist*, 90, 1827-1834.

458

459 Seidl, W., and Breu, J. (2005) Single crystal structure refinement of tetramethylammonium-
460 hectorite. *Zeitschrift für Kristallographie*, 220, 169-176.

461

462 Soler, J. M., Artacho, E., Gale, J. D., García, A., Junquera, J., Ordejón, P., and Sánchez-
463 Portal, D. (2002) The SIESTA method for ab-initio order-N materials simulation. *Journal of*
464 *Physics: Condensed Matter*, 14, 2745-2779.

465

466 Troullier, N., and Martins, J.L. (1991) Efficient pseudopotentials for plane-wave
467 calculations. *Physical Reviews B*, 43, 1993-2006.

468

469 Vahedi-Faridi, A., and Guggenheim, S. (1997) Crystal structure of tetramethylammonium-
470 exchanged vermiculite. *Clays and Clay Minerals*, 45, 859 – 866.
471

Captions of Figures

Figure 1. Arrangement of TMA molecules in the interlayer of vermiculite. Left: Vahedi-Faridi and Guggenheim model; Right: Seidl and Breu model. N, C, and H atoms of TMA are represented in green, grey and white balls respectively. O, Si, and Al atoms from vermiculite tetrahedral sheet are represented in red, yellow and purple respectively.

Figure 2. Cation arrangements of the (a) octahedral sheet, (b) upper tetrahedral sheet of 2:1 layer, (c) lower tetrahedral sheet of 2:1 layer (the TMA, which are close to the tetrahedral-ring cavities of the upper and lower tetrahedral sheets, are represented as blue triangles), and (d) lateral view of parts of the 2:1 layer and interlayer of vermiculite. The Mg, Al, Si, O, C, N and H atoms are in green, pink, yellow, red, black, blue, and light grey, respectively. Parts (b), (c) and (d) show the projections of the TMA cations for the initial HC1 model. (all TMA are dispersed, TMA cations which are in the front are highlighted as spheres). Parts (e) and (f) show the initial HC2 and HC3 models, respectively.

Figure 3. TMA orientations in the interlayer of the optimized vermiculite model HC1 (a), HC2 (b), and HC3 (c). The Mg, Al, Si, O, C, N and H atoms are in green, pink, yellow, red, black, blue, and light grey, respectively. The TMA cations are highlighted as balls.

Figure 4. Optimized vermiculite models with vermiculite + TMA + H₂O, LC-W4 (a) and montmorillonite + TMA + H₂O (b). The Mg, Al, Si, O, C, N and H atoms are in green, pink, yellow, red, black, blue, and light grey, respectively. TMA cations which are in the front are highlighted as spheres.

Figure 5. Density profiles, along the *c* axis of the interlayer, of the atoms in vermiculite-TMA models HC1 (bottom profile in a), LC-W4 (top profile in a) and LC-W1 (b); and the hydrated TMA-montmorillonite (c). Dashed black lines represent N atoms density; Black lines represent vermiculite atoms density; Grey dotted lines represent the interlayer cations N atoms density in the experimental crystal structure (Vahedi-Faridi and Guggenheim, 1997).

Figure 6. Density profile of the O atoms (in dashed line) of water molecules in the LC-W4 model (a) (solid line represents the profile of the tetrahedral and octahedral layers of vermiculite), and radial distribution functions of O...O (b), H...H (c), and O...H (d) distances of the water molecules in the interlayer of LC-W4 model.

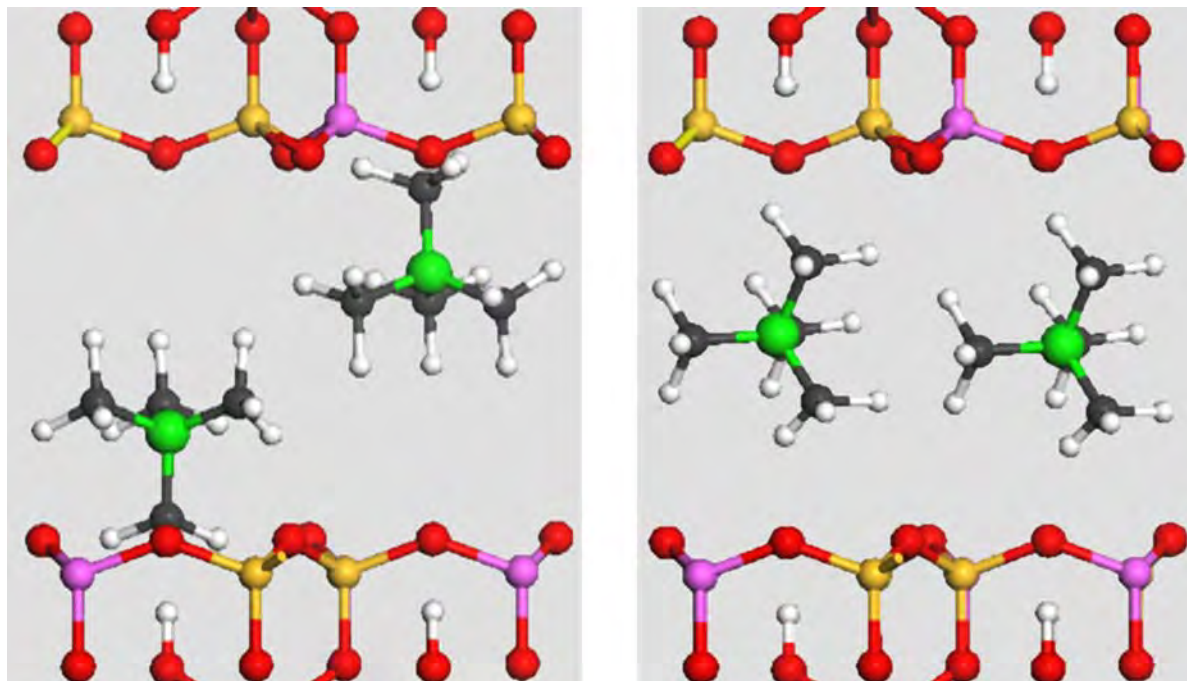


Fig 1.-

Fig. 2

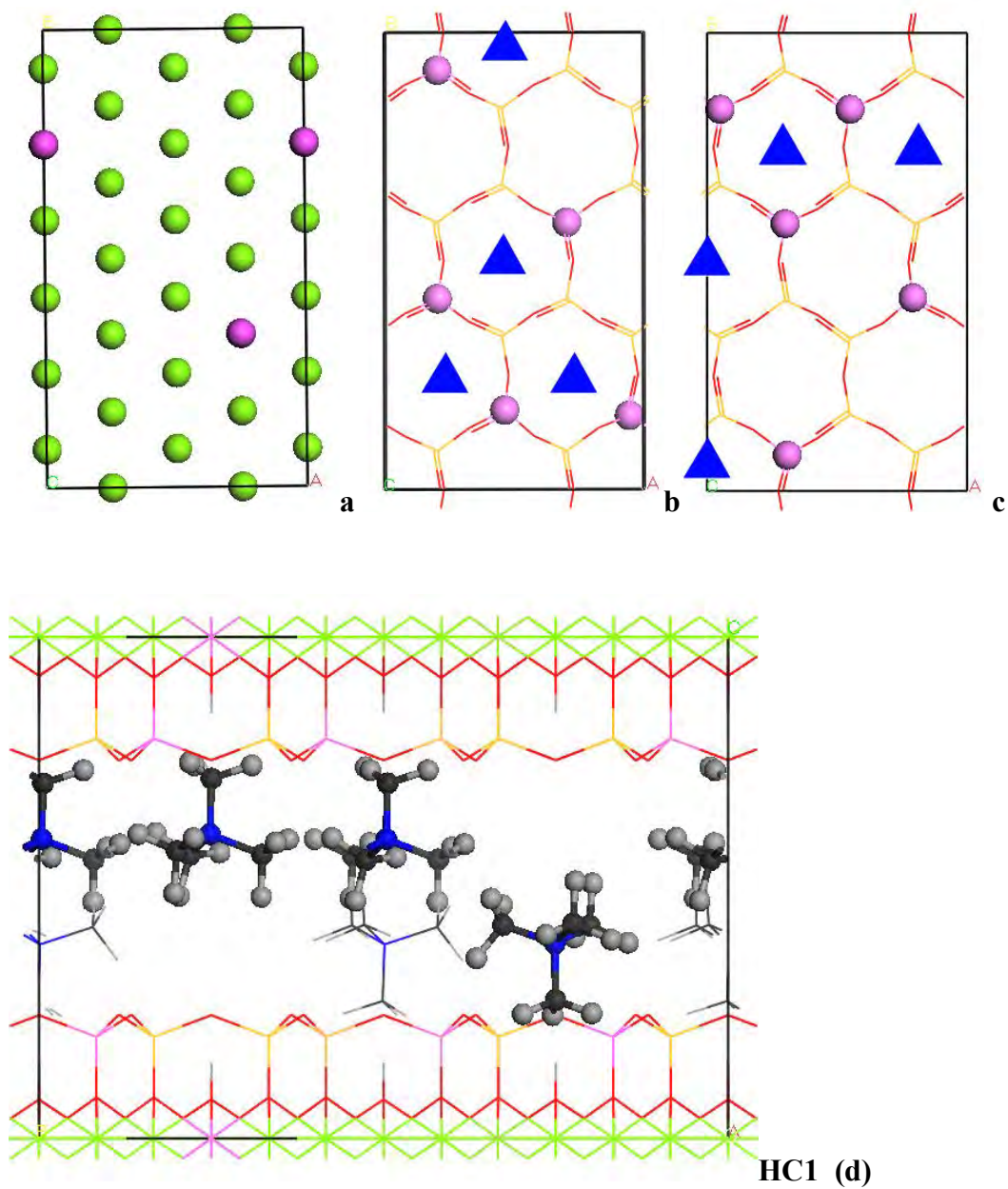
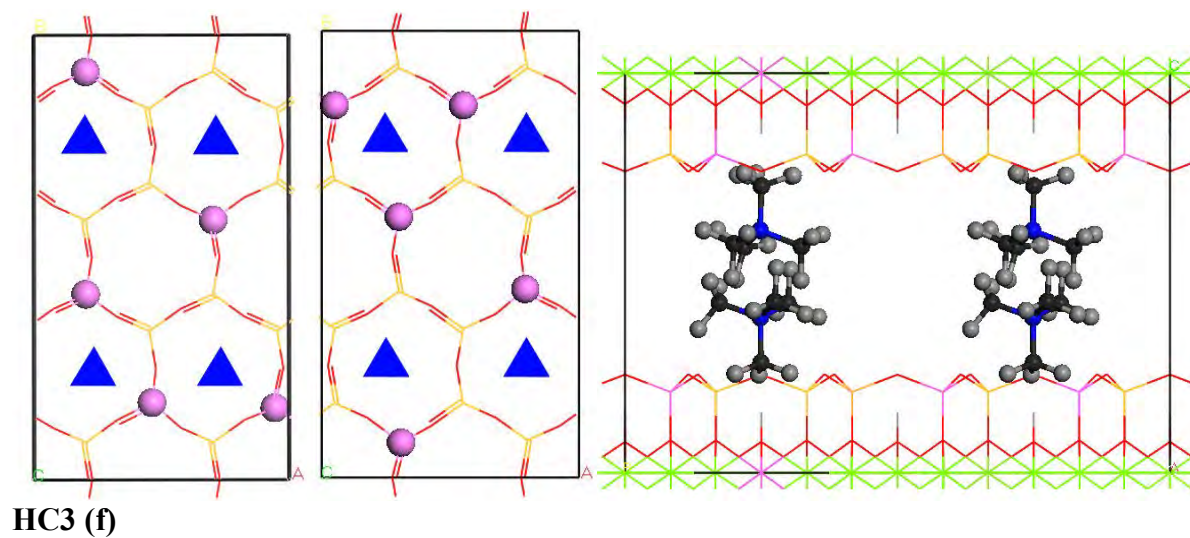
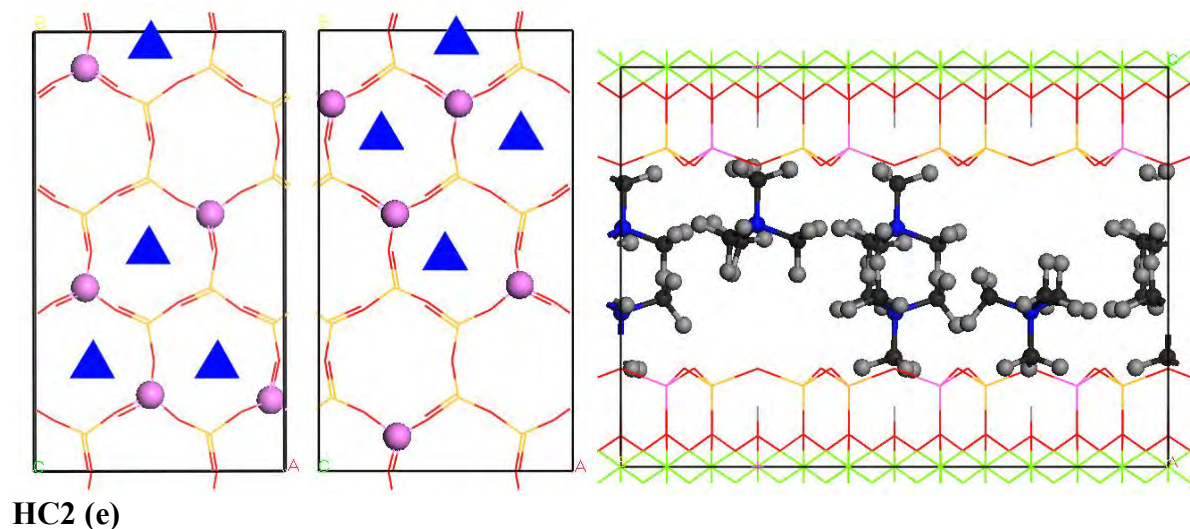
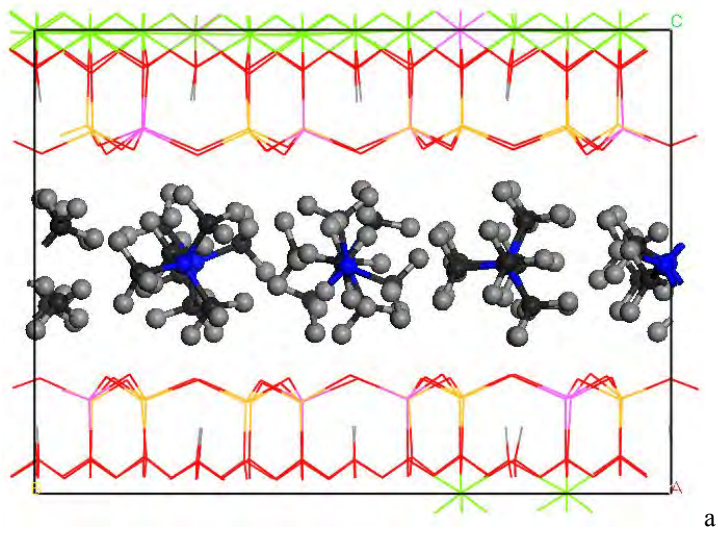
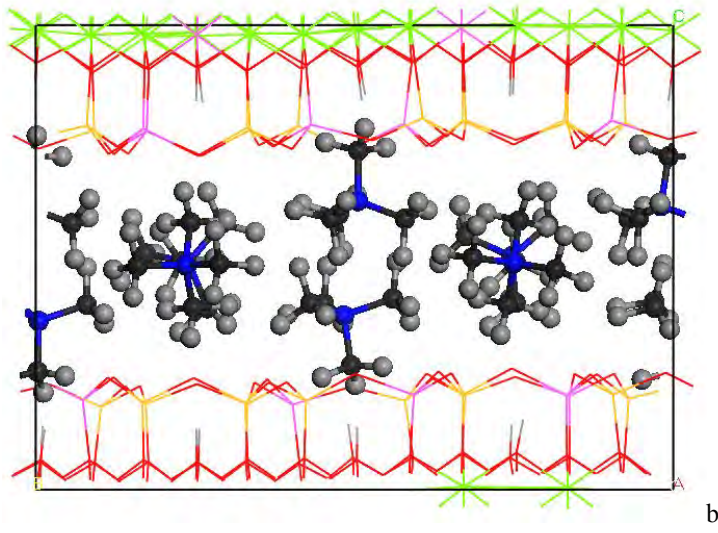


Fig 2 (cont.)

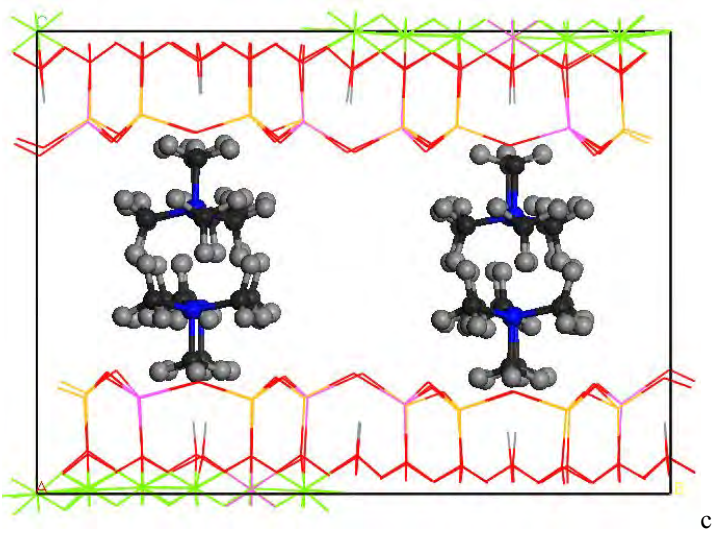




a



b



c Fig. 3.-

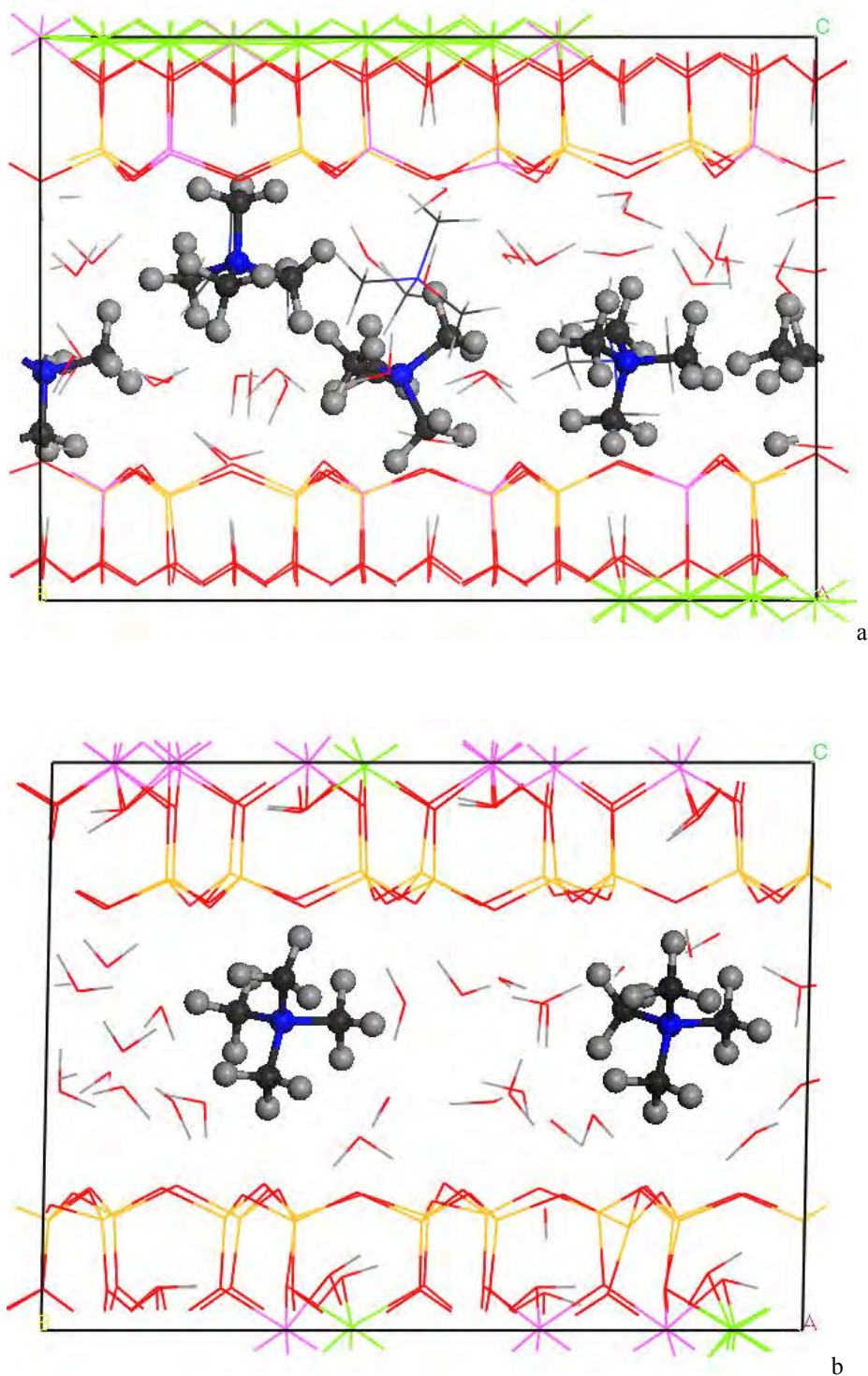
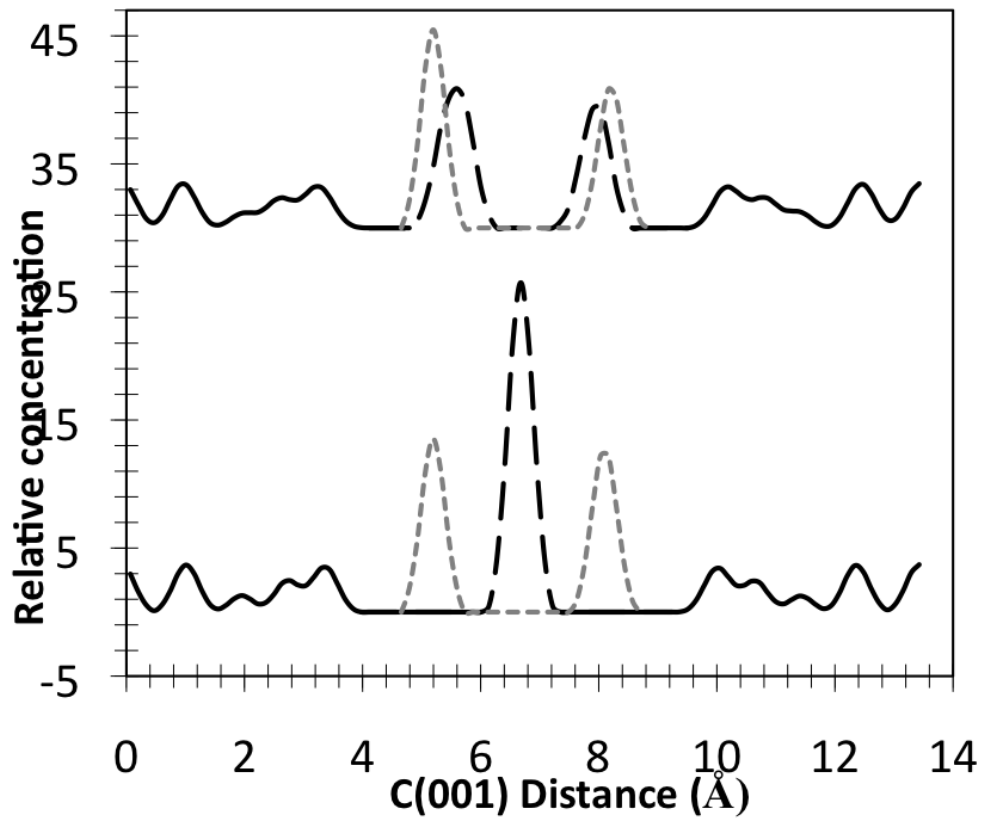
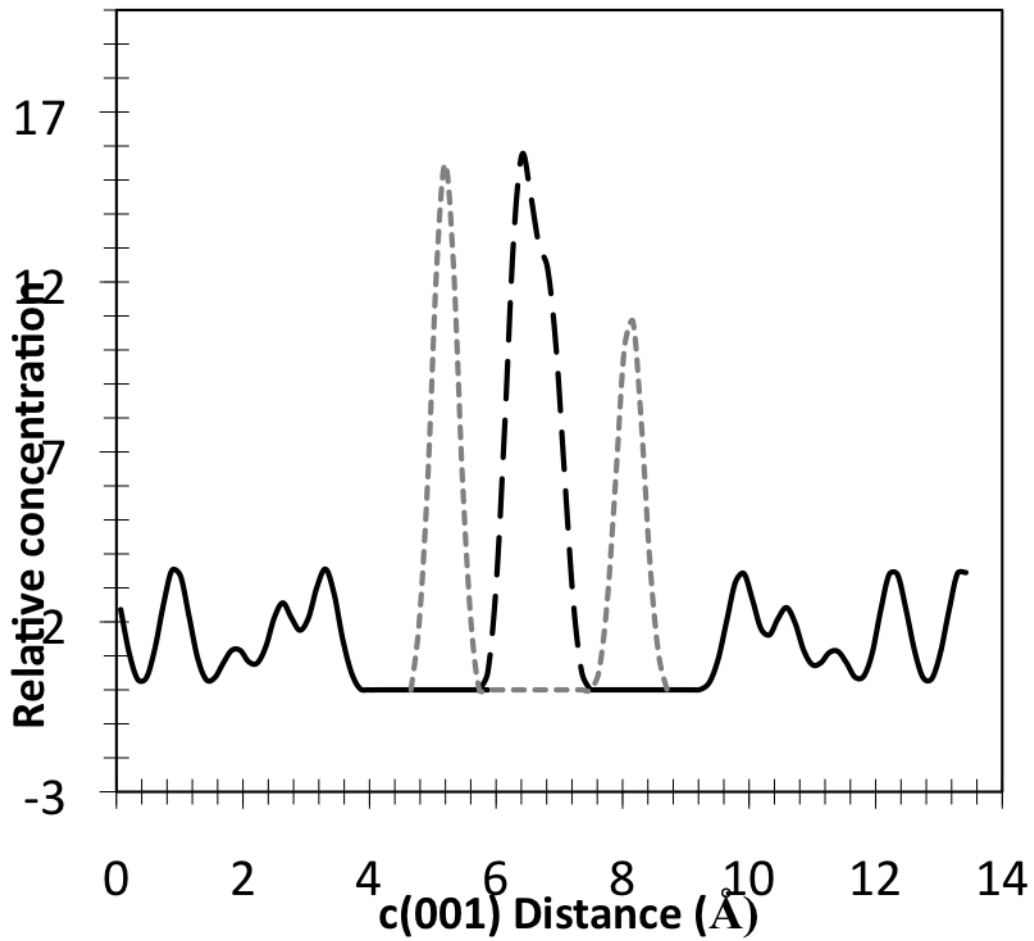


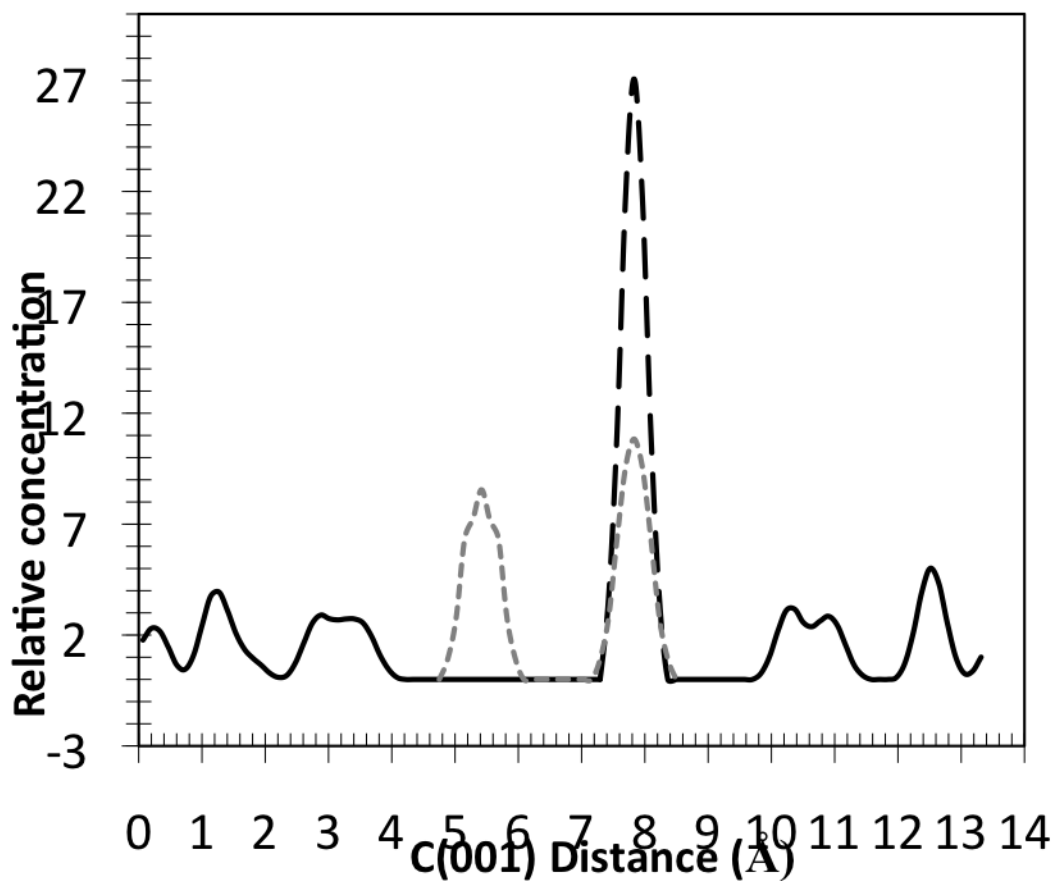
Fig. 4



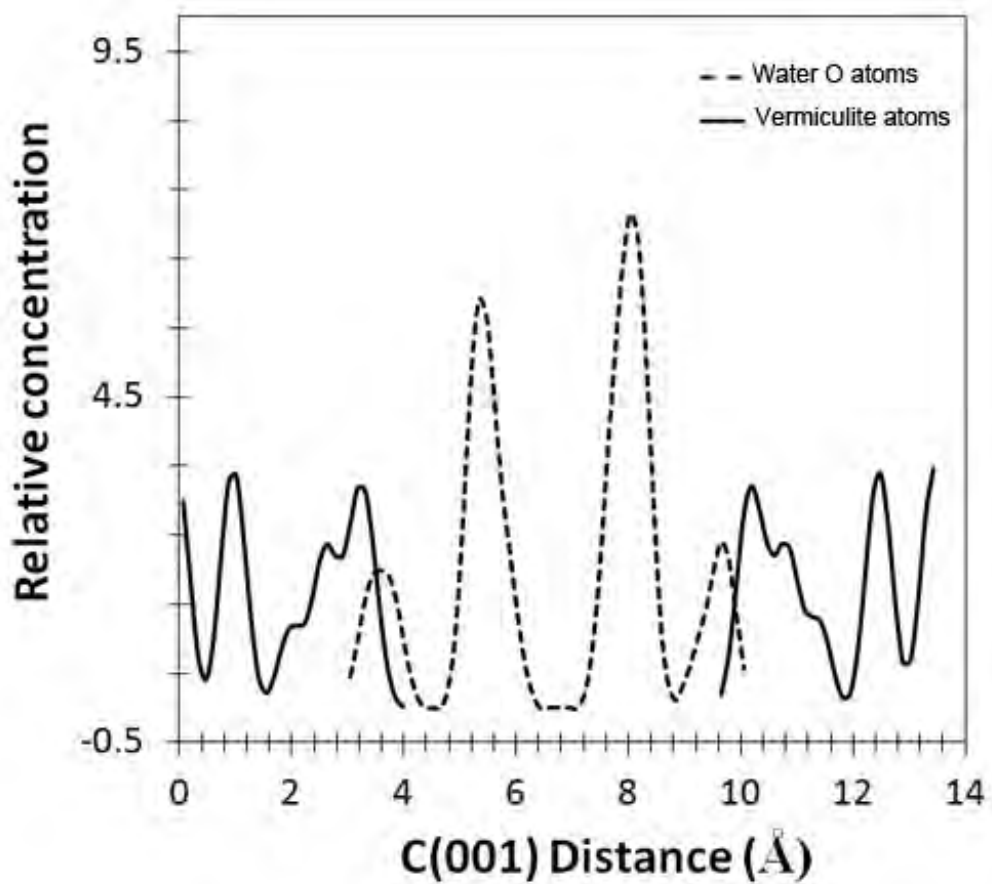
a



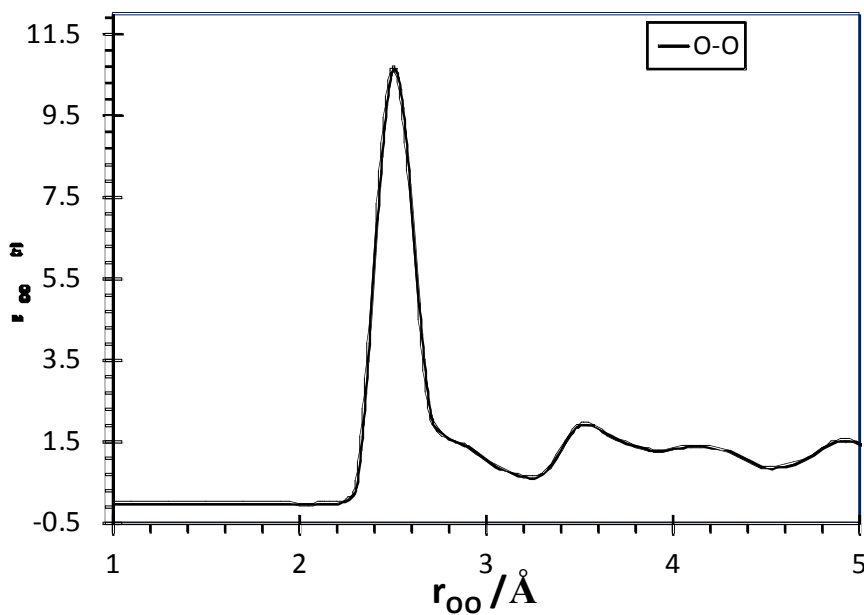
b



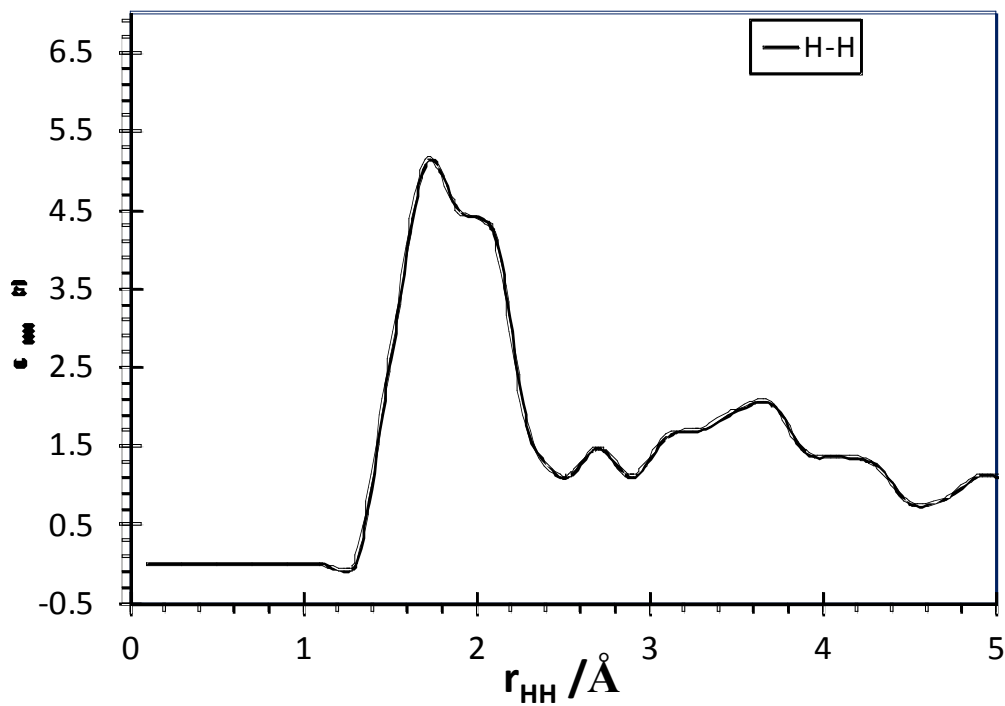
^c
Fig. 5.-



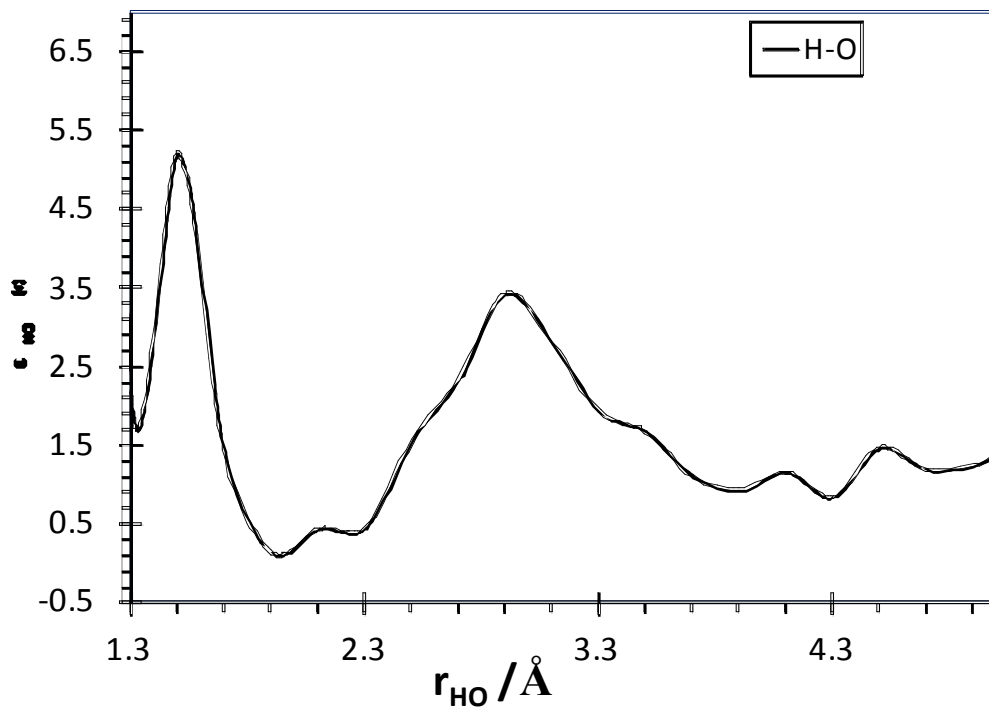
a



b



c



d

Fig. 6.-

Table 1.- Models of TMA-vermiculite complex and relative energy (in eV) within each group of samples.

sample	Unit cell formula	ΔE (eV)
VLC1	$TMA_{1.25}(Mg_5Al)(Si_{5.75}Al_{2.25})O_{20}(OH)_4$	0.0
VLC2	$TMA_{1.25}(Mg_5Al)(Si_{5.75}Al_{2.25})O_{20}(OH)_4$	18.22
HC1	$TMA_2(Mg_{5.5}Al_{0.5})(Si_{5.5}Al_{2.5})O_{20}(OH)_4$	0.0
HC2	$TMA_2(Mg_{5.5}Al_{0.5})(Si_{5.5}Al_{2.5})O_{20}(OH)_4$	16.88
HC3	$TMA_2(Mg_{5.5}Al_{0.5})(Si_{5.5}Al_{2.5})O_{20}(OH)_4$	37.70
HC4	$TMA_2(Mg_{5.5}Al_{0.5})(Si_{5.5}Al_{2.5})O_{20}(OH)_4$	16.79
LC-W1	$TMA_{1.75}(Mg_{5.25}Al_{0.75})(Si_{5.5}Al_{2.5})O_{20}(OH)_4(H_2O)_{2.25}$	
LC-W2	$TMA_{1.75}(Mg_{5.25}Al_{0.75})(Si_{5.5}Al_{2.5})O_{20}(OH)_4(H_2O)_{4.5}$	
LC-W3	$TMA_{1.75}(Mg_{5.25}Al_{0.75})(Si_{5.5}Al_{2.5})O_{20}(OH)_4(H_2O)_{6.75}$	
LC-W4	$TMA_{1.75}(Mg_{5.25}Al_{0.75})(Si_{5.5}Al_{2.5})O_{20}(OH)_4(H_2O)_{8.5}$	